Accepted Manuscript

Experimental investigation of stimulated Raman scattering effect in high-power nanosecond superfluorescent fiber source

Chaoyu Ning [1,2,3,4], Shuzhen Zou [1,4], Haijuan Yu [1,2,3,4], Jiexi Zuo [1,2,3,4], Xuechun Chen [1,2,3,4], Shuang Xu [1,2,3,4], Shifei Han [1,2,3,4], Xinyao Li [1,2,3,4], Wenjuan Wu [1,2,3,4], Chaojian He [1,4], and Xuechun Lin [1,2,3,4]

[1] *Laboratory of All-solid-state Light Sources, Institute of Semiconductors, Chinese Academy of Sciences, Beijing 100083, China*

[2] *Center of Materials Science and Optoelectronics Engineering, University of Chinese Academy of Sciences, Beijing 100049, China*

[3] *College of Materials Science and Opto-Electronic Technology, University of Chinese Academy of Sciences, Beijing 101407, China*

[4] *Beijing Engineering Technology Research Center of All-Solid-State Lasers Advanced Manufacturing, Beijing 100083, China*

Correspondence to: X. Lin, No. A35, Qing Hua East Road, Beijing 100083, China.
Email: xclin@semi.ac.cn

Chaoyu Ning and Shuzhen Zou contributed equally to this work and are co-first authors.

Abstract In this work, we experimentally investigate the dependence of the stimulated Raman scattering (SRS) effect on the seed’ s linewidth of high-power nanosecond superfluorescent fiber source (ns-SFS). The results reveal that the SRS in ns-SFS amplifier

This peer-reviewed article has been accepted for publication but not yet copyedited or typeset, and so may be subject to change during the production process. The article is considered published and may be cited using its DOI.

10.1017/hpl.2023.72

is significantly influenced by the full width at half maximum (FWHM) of the ns-SFS seed, and there is an optimal FWHM linewidth of 2 nm to achieve the lowest SRS in our case. The first-order SRS power ratio increases rapidly when the seed' s linewidth deviates from the optimal FWHM linewidth. By power-scaling ns-SFS seed with optimal FWHM linewidth, a narrowband all-fiberized ns-SFS amplifier is achieved with a maximum average power of 602 W, pulse energy of 24.1 mJ, and corresponding peak power of 422.5 kW. This is the highest average power and pulse energy for all-fiberized ns-SFS amplifiers to the best of our knowledge.

Key words: nanosecond superfluorescent fiber source, stimulated Raman scattering effect, fiber amplifier, high power

I. Introduction

Pulsed fiber lasers with conspicuous conversion efficiency, compactness, and reliability have gained widespread attention in laser processing, nonlinear frequency conversion, coherent beam combining, and other applications [1-4]. Especially, the all-fiberized nanosecond pulsed amplifiers with high power and large energy are desired in varied applications such as laser ablation and surface treatments [5, 6]. Typically, high-power all-fiberized nanosecond pulsed amplifiers employ a master oscillator power amplifier (MOPA) configuration where the nanosecond fiber seed is achieved via Q-switched regime or external modulation of a continuous-wave fiber laser [7, 8]. However, the stochastic self-pulsing and the interactions of longitudinal modes inherent in fiber oscillators degrade their temporal stability and the threshold of the nonlinear effects, thereby limiting the average power and pulse energy of all-fiberized pulsed amplifiers [8-10]. Additionally, all-fiberized nanosecond pulsed amplifiers with low coherence are demanded in the high-quality

https://doi.org/10.1017/hpl.2023.72 Published online by Cambridge University Press

full-field imaging of dynamic targets on nanosecond timescale and other applications [11]. Therefore, it is significant to develop a fiber seed that improves temporal stability and unlocks the application potential of high-power nanosecond pulsed amplifiers.

The superfluorescent fiber source (SFS) derives from the superfluorescent radiation in the active fiber, which has unique features such as broadband emission, low coherence, and high temporal stability [12-14]. The pursuit of high-power SFS amplifiers has emerged as a research frontier, owing to their potential for diverse applications such as the generation of mid-infrared laser and supercontinuum sources, the pumping of Raman fiber lasers, and material processing [15-17]. Due to the absence of resonant cavity structure, the SFS can effectively avoid the self-pulsing and the interactions of longitudinal modes, improving the temporal stability and exhibiting remarkable advantages in nonlinear effects suppression [18-21]. Thus, the nanosecond fiber seed generated by externally modulated SFS can resolve the temporal instability issues associated with the resonant cavity structure-based nanosecond fiber seed. However, demonstrations of high-power SFS amplifiers have predominantly focused on continuous-wave SFSs [22-26], with reports on pulsed SFS amplifiers featuring high average power and large pulse energy being relatively scarce. E J Park et al. [19] reported a narrowband ns-SFS with an average power of 41.5 W, pulse energy of about 0.4 mJ, and pulse width of 26.4 ns, while pulsed SFS amplifiers delivering average power in the hundred-watt level and pulse energy in the ~10 mJ level have yet to be reported. In addition, the scaling of average power and pulse energy in all-fiberized nanosecond amplifiers is primarily limited by amplified spontaneous emission (ASE) and nonlinear effects, particularly the SRS [27]. And recent research indicates that the SRS in continuous-wave fiber lasers is significantly related to the spectral width. For instance, T. Schreiber et al. [28] reported that the threshold of SRS for fiber oscillators depends on the spectral width of the out-coupling fiber Bragg grating (FBG),

https://doi.org/10.1017/hpl.2023.72 Published online by Cambridge University Press

while Liu W et al. [29] demonstrated that the SRS in narrowband filtered SFS is enhanced rapidly with the narrowing of seed's linewidth. Besides, V. Bock et al. [30] fully explained the observed SRS enhancement for spectrally narrower fiber laser systems. Hence, investigating spectral evolution to inhibit SRS is a promising approach for achieving high output power and large pulse energy of all-fiberized ns-SFS amplifiers.

In this work, we obtain the nanosecond fiber seed by externally modulated SFS and investigate the impact of the seed' s linewidth on SRS in an ns-SFS amplifier for the first time. Our experimental findings indicate that the SRS in the ns-SFS amplifier is significantly influenced by the FWHM linewidth of the ns-SFS seed. Specifically, when the seed' s linewidth is less than or greater than 2 nm, the first-order SRS power ratio in the ns-SFS amplifier grows rapidly at a specific pump power. Since the ns-SFS seed with a FWHM linewidth of 2 nm exhibits the best SRS suppression, we amplify its average power and pulse energy. At this point, the amplified ns-SFS attains a maximum average power of 602 W, a pulse width of 57 ns, a pulse energy of 24.1 mJ, and a peak power of 422.5 kW. This is the highest average power and pulse energy for all-fiberized ns-SFS amplifiers ever reported.

II. Experimental setup

2.1. The nanosecond pulsed superfluorescent fiber source

The experimental setup utilized in this study comprises a typical MOPA configuration, mainly comprising a low-power ns-SFS seed and three-stage amplifiers. As shown in Fig. 1, the ns-SFS seed consists of a superfluorescent fiber source, a pre-amplifier, and a spectral filtering cell. The SFS is pumped by a 9 W 976 nm laser diode (LD). The pumping light is coupled into an 11 m double-cladding Yb-doped fiber (YDF) using a (2+1) ×1 signal/pump combiner. The active fiber

https://doi.org/10.1017/hpl.2023.72 Published online by Cambridge University Press

has a core diameter of 10 μm, an inner cladding diameter of 125 μm, and a cladding absorption coefficient of 1.65 dB/m at 915 nm. The end of the backward output is cleaved at an 8° angle to reduce the feedback along the fiber. In the meantime, the forward output of the SFS is modulated by an acoustic-optical modulator (AOM 1) to generate nanosecond pulses. After the AOM 1, the generated nanosecond pulses are directed into the pre-amplifier via a (2+1) ×1 signal/pump combiner, where the active fiber has the same parameters as the SFS and is 6 m in length. A 976 nm LD also pumps the pre-amplifier with a maximum power of 9 W. The amplified nanosecond pulses are then launched into AOM 2, the same as AOM 1, to enhance the extinction ratio. Notably, AOM 1 and AOM 2 are synchronized by an arbitrary waveform generator (AWG). The spectrum of the pulsed SFS is modulated in the spectral filtering cell after the AOM 2. In the spectral filtering cell, three schemes are implemented. Scheme A allows the pulsed SFS to pass only through a circulator (CIR) without spectral filtering. Scheme B employs a bandpass filter (BP) to achieve the pulsed SFS with an FWHM linewidth of 8 nm, while Scheme C utilizes fiber Bragg grating (FBG) with different linewidths to obtain pulsed SFS with an FWHM linewidth of 0.25 nm, 0.5 nm, 1 nm, 2 nm, 3 nm, 5 nm. In addition, fiberized isolators (ISO) and homemade cladding pump strippers (CPS) are used in each stage to safeguard the preceding stage and dump the light in the cladding.

https://doi.org/10.1017/hpl.2023.72 Published online by Cambridge University Press

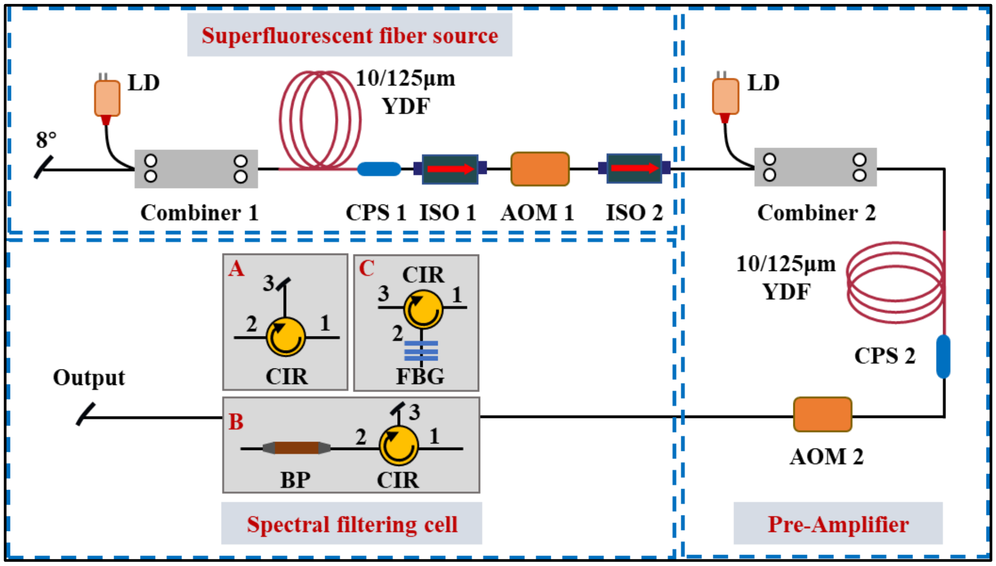

Fig. 1. The experimental setup of the ns-SFS seed.

Experimentally, by employing the AWG to set the drive signals of AOM 1 and AOM 2, the ns-SFS with a pulse width of 255 ns and repetition frequency of 25 kHz is generated after the pre-amplifier. The spectrum of the ns-SFS is then manipulated in the spectral filtering cell. Fig. 2(a) illustrates that the spectral range of the unfiltered ns-SFS spans from 1025 nm to 1123 nm, featuring a central wavelength of 1069.8 nm and an FWHM of 14 nm. Additionally, the spectra of ns-SFS filtered by schemes B and C are shown in Fig. 2(b), where the legend represents the FWHM linewidth of the filtered spectrum, with all filtered ns-SFSs having a central wavelength of approximately 1064 nm. Furthermore, Fig. 2(c) demonstrates that the intensity-normalized pulse profiles of the unfiltered ns-SFS and filtered ns-SFSs are nearly identical, exhibiting a pulse width of ~ 255 ns. However, the peak of the pulse profiles exhibits different temporal fluctuations. And the pulse peaks in Fig. 2(c) are separated by intensity bias to illustrate the details of the fluctuations at the pulse peak of the ns-SFS seed, as shown in Fig. 2(d). The results indicate that the temporal fluctuations of the pulse peak are weak when the FWHM linewidth is larger than 2 nm but are significantly strengthened when the FWHM linewidth is smaller than 2 nm. Thus, the wideband ns-SFS seed can effectively resolve the issues such as self-pulsing commonly observed in

https://doi.org/10.1017/hpl.2023.72 Published online by Cambridge University Press

oscillator-based fiber seeds [9, 10], while extensive spectral filtering also leads to a degradation in the temporal stability of ns-SFS seed.

Moreover, the average power of ns-SFS obtained by AOM 1 modulation is 2.3 mW. After the pre-amplifier and spectral filtering cell, the average output power of unfiltered ns-SFS is amplified to around 445 mW. However, the spectral narrowing of the seed by spectral filtering results in average power loss, yielding the output power ranges from 133.1 mW for an 8 nm ns-SFS to 3.0 mW for a 0.25 nm ns-SFS (see details in Table 1).

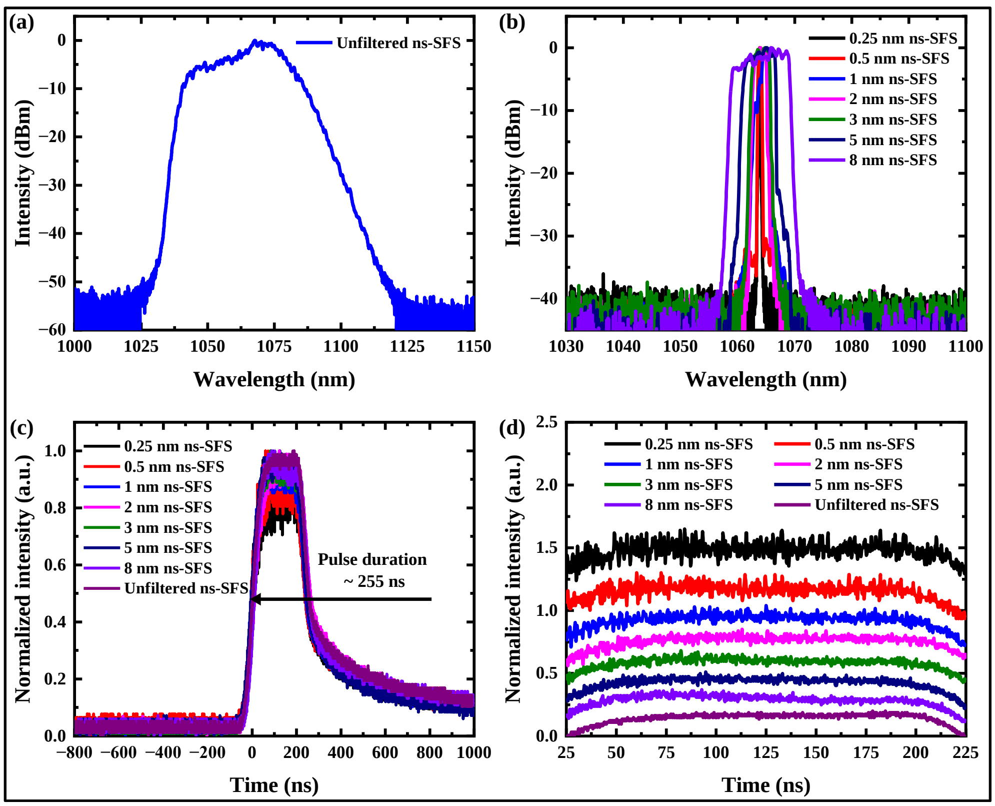

Fig. 2. The output characteristics of ns-SFS seed. The output spectra of the unfiltered ns-SFS (a) and the filtered ns-SFSs (b). (c) The pulse profiles, and (d) the fluctuations at the pulse peak of the ns-SFS seed.

Table 1. Output power of ns-SFS seed vs. FWHM linewidth

Seed linewidth (nm)	Output power (mW)	Seed linewidth (nm)	Output power (mW)

https://doi.org/10.1017/hpl.2023.72 Published online by Cambridge University Press

unfiltered ns-SFS	445.0	2	22.4
8	133.1	1	11.5
5	36.6	0.5	5.7
3	30.8	0.25	3.0

2.2. The power amplifiers

To further increase the output power of ns-SFS, the pulses are injected into two booster amplifiers for preamplification, and finally power amplified by a main amplifier (see Fig. 3). The components used in the first booster amplifier are the same as those used in the pre-amplifier of ns-SFS seed except for the absence of an AOM and the utilization of a 2.5 m-long active fiber in the first booster amplifier. The second booster amplifier is constructed using a 2.8 m long YDF with core/inner cladding diameters of 30/250 μm, pumped by a 60 W fiber pigtailed 976 nm LD through a (2+1) ×1 signal/pump combiner. For the main amplifier, a 2 m long YDF is employed with core/inner cladding diameters of 100/400 μm (core NA=0.11, absorption coefficient of approximately 6 dB/m at 915 nm). Six 976 nm LDs with a maximum output power of 180 W are used to pump the active fiber of the main amplifier via a (6+1) ×1 signal/pump combiner. Besides, to better investigate the influence of the ns-SFS seed' s FWHM linewidth on SRS, a 15 m-long passive fiber (GDF) matched with the active fiber of the main amplifier in size is employed to heighten the SRS. A fiber-pigtailed end cap is applied at the end of the system to avoid unexpected end reflection and fiber facet damage. Meanwhile, the ISO and CPS are arranged at every stage to protect the preceding stage from damaging and dump the residual pump light. Apart from the fiber pigtailed end cap, all the other optical components are mounted on water-cooled heat sinks.

In our all-fiberized ns-SFS MOPA system, the following instruments are utilized to characterize its performance: a water-cooled power meter to measure the average power, a digital oscilloscope (KEYSIGHT MSOX3104T) with a sampling rate of 5 GS/s to observe the pulse

https://doi.org/10.1017/hpl.2023.72 Published online by Cambridge University Press

profile, and an optical spectrum analyzer (YOKOGAWA AQ6370D) with a minimum resolution of 0.02 nm to analyze the amplified ns-SFS spectra.

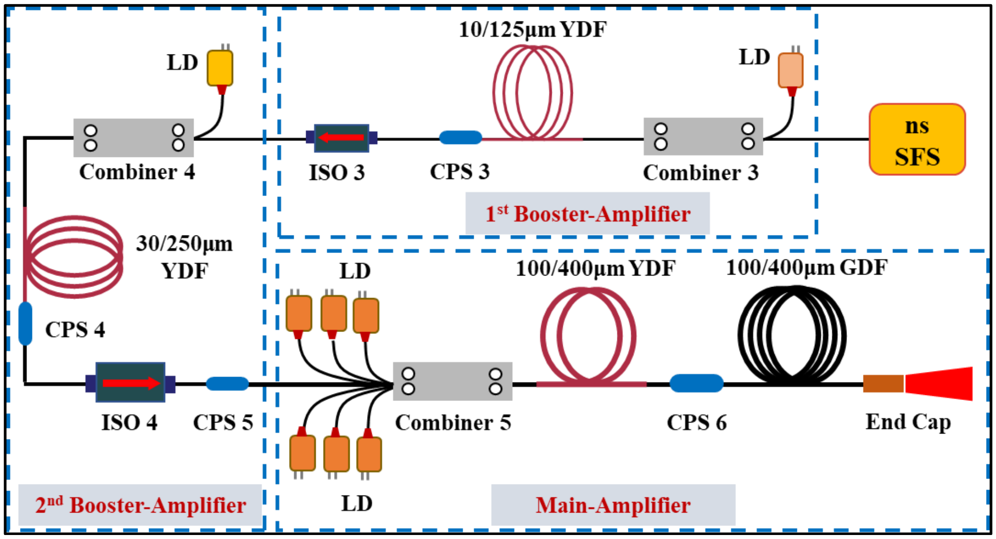

Fig. 3. The experimental setup of ns-SFS amplifier.

III. Results and discussion

3.1. SRS effect in the ns-SFS amplifier with various seed' s linewidths

3.1.1. Amplification of ns-SFS seed with different linewidths

To study the amplification characteristics and the SRS inhibition ability of ns-SFS seed with different FWHM linewidths, we experimentally investigate the power scaling of the filtered ns-SFS seeds. To ensure the accuracy of the results, we first compare the output characteristics of the booster amplifiers. All filtered ns-SFS seeds have a repetition frequency of 25 kHz and a pulse width of ~255 ns (see Fig. 2(c)). The average output power of the filtered ns-SFSs can be amplified to 1 W by the first booster amplifier and then be amplified to about 18 W by the second booster amplifier. The spectra of the amplified ns-SFS with an output power of 18 W after two booster amplifiers are shown in Fig. 4(a). The central wavelength of all filtered ns-SFS signals is remained at about 1064 nm, while the spectral range is significantly widened due to the onset of nonlinear

https://doi.org/10.1017/hpl.2023.72 Published online by Cambridge University Press

effects such as the SPM. On the other hand, as shown in Fig. 4(b), the pulse profiles of the amplified ns-SFSs with an average power of 18 W are nearly identical, whose pulse widths are compressed from ~255 ns to ~100 ns owing to pulse distortion [31]. Therefore, the filtered ns-SFS signals have similar pulse profile, pulse width, output power, and pulse energy before entering the main amplifier, which can ensure the reliability of the results of amplified ns-SFS signals in the main amplifier.

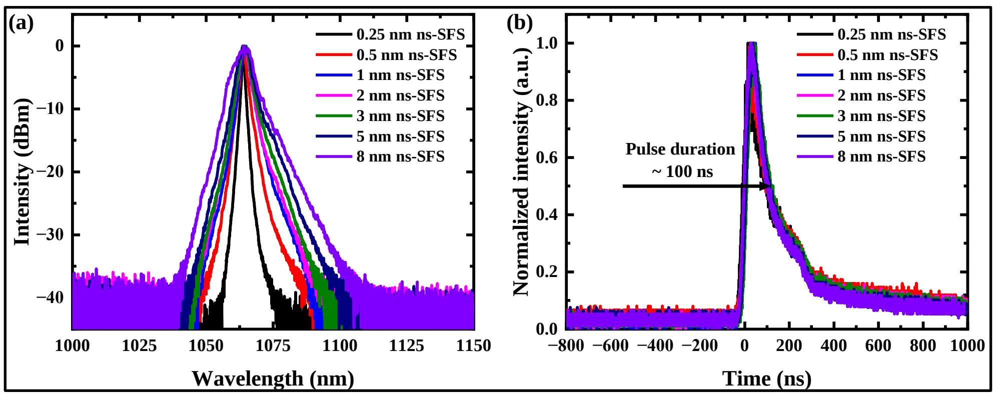

Fig. 4. The output spectra (a) and the pulse profiles (b) of the ns-SFS signals at an output power of ~ 18 W.

After the first and second booster amplifiers, we inject 18 W output power of filtered ns-SFSs into the main amplifier as the signal to explore power scalability and SRS effect. In Fig. 5(a), it can be observed that the output power of the ns-SFS signals grows linearly as the pump power increases in all cases. Specifically, a maximum average power of about 265 W is achieved at a pump power of 370 W for all filtered ns-SFS signals, resulting in an optical-to-optical efficiency of about 68% and a pulse energy of about 10.6 mJ. The further power scaling of these ns-SFS signals is restricted by the SRS, which is enhanced by the long passive-matched fiber (see Fig. 6 for details). The low optical-to-optical efficiency of the ns-SFS signals can be attributed to the transfer of the signal power to the Raman Stokes light. Fig. 5(b) displays the pulse width of the amplified ns-SFSs versus the pump power. The pulse width of the signals entering the main

https://doi.org/10.1017/hpl.2023.72 Published online by Cambridge University Press

amplifier is nearly identical for all cases, with the value of about 100 ns. And the maximal deviation of the pulse widths between the highest and lowest values is less than 2.5 ns. As the pump power increases, the pulse width of the seven ns-SFS signals gradually narrows. At a pump power of 370 W, the pulse duration of the seven ns-SFS signals is narrowed to about 67 ns with a maximal deviation of less than 1.0 ns. Fig. 5(c) presents the pulse profiles of the seven ns-SFS signals at a pump power of 370 W. Although there is a slight difference in pulse width after amplification, the pulse profiles remain essentially the same, exhibiting a steeper leading edge than the trailing edge. Additionally, the temporal fluctuations of the pulse peak are stronger with the spectral narrowing of the filtered ns-SFSs at the pump power of 370 W, as demonstrated in Fig. 5(d). At the maximum average power, the peak power for the seven ns-SFS amplifiers fluctuates slightly around 158 kW, with a maximum deviation of less than 4 kW between the highest and lowest values. Considering that the seven ns-SFS amplifiers exhibit nearly identical average power, pulse width, and pulse profile under the same pump power, their peak power density remains almost identical.

https://doi.org/10.1017/hpl.2023.72 Published online by Cambridge University Press

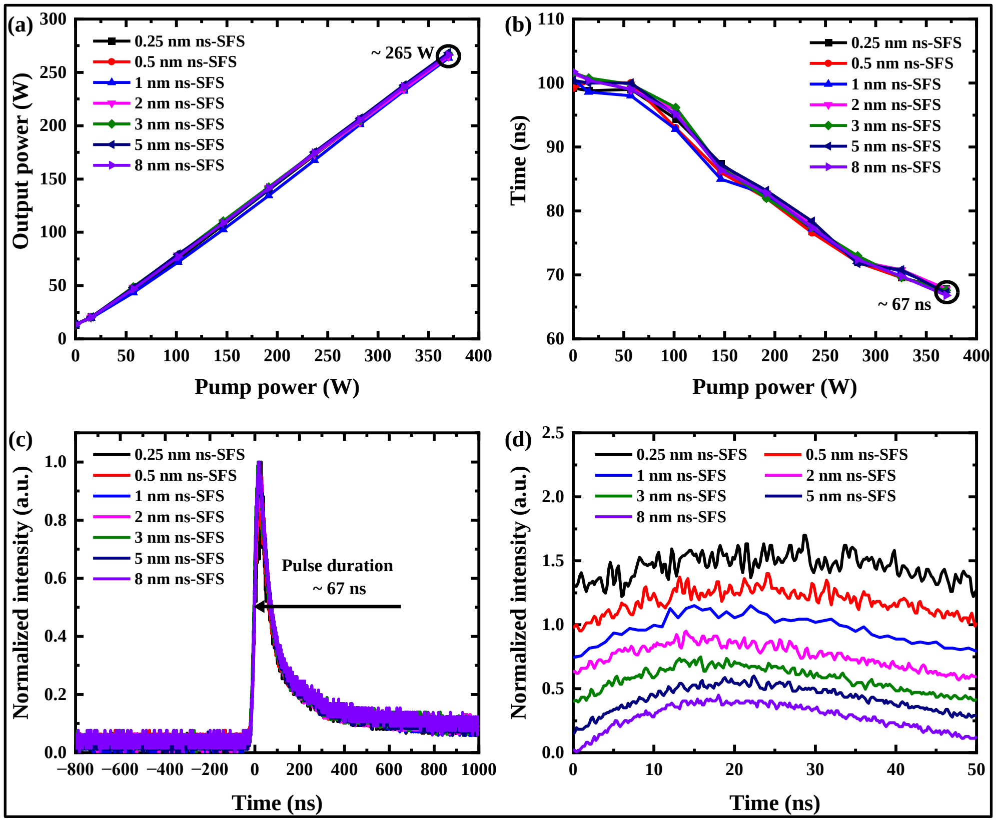

Fig. 5. (a) The output power and (b) pulse width of amplified ns-SFS signals as a function of pumping power, (c) the pulse profiles and (d) the details of the pulse peak of amplified ns-SFS signals at a pump power of 370 W.

3.1.2. The dependence of SRS on seed' s linewidth in ns-SFS amplifier

We analyze the Raman power ratio of seven ns-SFS amplifiers at varying pump powers to investigate the impact of the spectral FWHM linewidth on SRS. The strength of the SRS in laser with different cases cannot be accurately judged only by observing the intensity of the Raman peak, one has to take into account of the SRS wavelength band by spectral integration to calculate its proportion in the total laser output. Specially, we selected the spectral range of 1100 nm to 1150 nm as the first-order Raman Stokes light and calculated the first-order Raman power ratio of the seven ns-SFS amplifiers via dividing the integrated Raman spectrum by the integral spectrum from 1000 nm to 1220 nm as depicted in Fig. 6 (a). The results indicate that the first-order Raman power

https://doi.org/10.1017/hpl.2023.72 Published online by Cambridge University Press

ratio of the seven amplifiers increases rapidly with the growing pump power. Notably, at the same pump power, the 2 nm ns-SFS amplifier displays the lowest first-order Raman power ratio, whereas the Raman power ratio of ns-SFS amplifiers with seed’ s linewidth greater than or less than 2 nm is progressively enhanced.

To investigate the relationship between the SRS and the FWHM linewidth of the ns-SFS seed in more detail, we analyze the output spectra of ns-SFS amplifiers and the content of each spectral component under a pump power of 370 W, as depicted in Fig. 6(b) to Fig. 6(d). Fig. 6(b) shows the output spectra of the seven ns-SFS amplifiers at a pump power of 370 W. Because of the combination of the SPM and SRS enhanced by long passive matching fiber, all seven ns-SFS amplifiers exhibit severe asymmetric broadening in the output spectra, as compared to the 18 W signals entering the main amplifier (see Fig. 4(a)). The seven amplifiers manifest different first-order SRS content in the spectral range of 1100 nm to 1150 nm and second-order SRS content in the 1150 nm to 1220 nm range, respectively. Additionally, the ASE of all ns-SFS amplifiers at 1010 nm to 1045 nm is weak.

However, the spectral broadening of the amplified laser exhibits an overlap with the SRS peak, particularly evident in the case of the 8 nm ns-SFS. To enhance the accuracy of the SRS power ratio, one potential approach involves fitting the red wavelength shoulder of the spectral broadening to establish a baseline and subsequently integrating only the portion above this baseline. Fig. 6(c) shows the output spectra obtained experimentally and through fitting in the case of the 8 nm ns-SFS at a pump power of 370 W. In this instance, a first-order SRS wavelength band spanning 1100 nm to 1150 nm is fitted to establish a baseline.

According to the above method, we get an accurate first-order SRS power ratio. The dependence of the first-order SRS power ratio on the linewidth of ns-SFS seed at a pump power

https://doi.org/10.1017/hpl.2023.72 Published online by Cambridge University Press

of 370 W is shown in Fig. 6(d). Although the peak power of all seven ns-SFS amplifiers is approximately 158 kW, their first-order SRS power ratio increases rapidly when the seed’ s linewidth deviates from 2 nm. When the FWHM linewidth of the ns-SFS seed is less than 2 nm, the first-order SRS power ratio increases rapidly with the narrowing of the spectral width, consistent with the report in ref. [28-30, 32]. This phenomenon may be related to the temporal fluctuations at the pulse peak of the filtered ns-SFS seed, as reported in a previous study of SRS in narrowband SFS amplifier [29]. The temporal fluctuations at the pulse peak of ns-SFS seed and the main amplifier become significantly stronger when the seed’ s linewidth is less than 2 nm (see Fig. 2 (d) and Fig. 5(d)). The SRS effect is closely related to the temporal characteristics of the laser, and the temporal fluctuations can increase the effective Raman gain coefficient, resulting in the early onset of the first- and second-order Stokes waves [33, 34]. Therefore, these unstable pulse peaks cause the ns-SFS amplifier with a FWHM linewidth less than 2 nm to experience more severe SRS.

Conversely, the first-order SRS power ratio increases quickly with the broadening of the spectral width as the linewidth of ns-SFS seed is larger than 2 nm (see Fig. 6(d)), in which case the fluctuations at the pulse peaks of the ns-SFS seeds and amplifiers are weak (see Fig. 2(d) and Fig. 5(d)). We attribute this phenomenon to the impact of the severe SPM induced by the high peak power density of ns-SFS amplifiers on the SRS. The severe SPM results in a rapid spectral expansion on both wings of the central wavelength, even extending to the Raman wavelength band [35]. When the signal carrying the noise of the Raman wavelength band is amplified in the main amplifier, the SRS threshold will be reduced, leading to severe SRS [36, 37]. It can be seen from Fig. 4(a) that the wider the ns-SFS seed’ s FWHM linewidth, the wider the spectral range of the amplified 18W signals due to the SPM. This indicates that the signals entering the main amplifier

https://doi.org/10.1017/hpl.2023.72 Published online by Cambridge University Press

possess varying initial Raman band content. The first-order SRS ratio at a pump power of 0 W in Fig. 6(a) represents the initial Raman band content of the signals entering the main amplifier, with values of 0.01%, 0.02%, 0.04%, and 0.06% for the 2 nm ns-SFS, the 3 nm ns-SFS, the 5 nm ns-SFS, and the 8 nm ns-SFS, respectively. Although the initial Raman band content of these ns-SFS signals is very low, these noise levels can affect the SRS in the main amplifier, as reported in ref. [37]. Consequently, in the case that the linewidth of ns-SFS seed is greater than 2 nm, the spectral range of the ns-SFS signal with a wider linewidth expands more easily to the first-order Raman wavelength band than that of the narrow signal (> 2 nm) due to the SPM effect, resulting in higher noise content of the first-order Raman band in signal and more severe first-order SRS after power scaling.

We also investigate the relationship between the second-order SRS power ratio and the ns-SFS seed' s linewidth, as shown in Fig. 6(d). Here, the ratio of the second-order SRS power to the output power is calculated through dividing the integrated spectrum from 1150 nm to 1220 nm by the integrated spectrum from 1000 nm to 1220 nm. The second-order SRS power ratio decreases rapidly with the increase of linewidth and the value approaches 0 until the linewidth is larger than 2 nm. This may be related to the pulse peak' s fluctuations of the ns-SFS seeds and amplifiers rapidly weaken with the growing linewidth when the linewidth is less than 2 nm (see Fig. 2(d) and Fig. 5(d)). Then, the pulse peak' s fluctuations show a slight change towards wider linewidth.

https://doi.org/10.1017/hpl.2023.72 Published online by Cambridge University Press

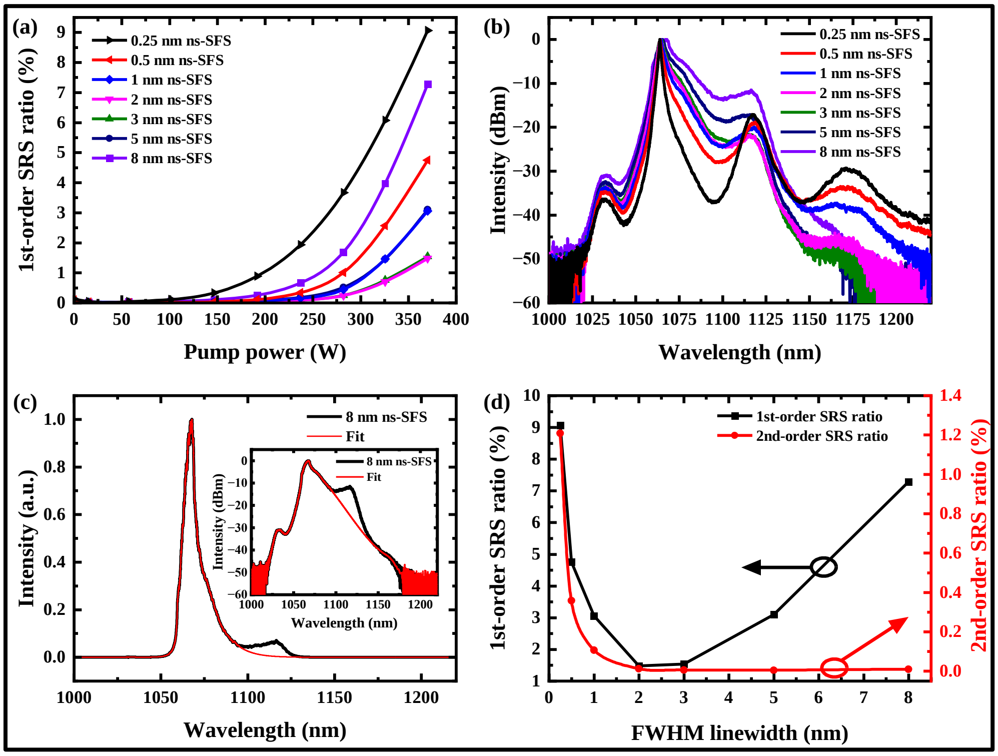

Fig. 6. The SRS of amplified ns-SFS with various linewidths. (a) The first-order SRS power ratio of seven ns-SFS amplifiers under different pump powers. (b) The output spectra of the ns-SFS amplifiers in a logarithmic scale with a pump power of 370 W. (c) The experimental and fitted output spectra in the case of 8 nm ns-SFS at a pump power of 370 W in a linear scale, insert: the corresponding spectra in a logarithmic scale for comparison. (d)The first-order SRS power ratio and the second-order SRS power ratio versus the ns-SFS seed' s FWHM linewidth at a pump power of 370 W.

In addition, the power ratio of the ASE light to total output is calculated by dividing the integrated spectrum from 1010 nm to 1045 nm by the integrated spectral range from 1000 nm to 1220 nm, which is called the ASE ratio for short. The dependence of the ASE ratio and spectral broadening factors on the seed' s FWHM linewidth at a pump power of 370 W is shown in Fig. 7. As the linewidth of the ns-SFS seed increases, the ASE ratio gradually decreases from 0.13% to

https://doi.org/10.1017/hpl.2023.72 Published online by Cambridge University Press

0.08%, which may be caused by the wideband ns-SFS signal consuming more inverted population than the narrowband signal. Notably, the ASE power ratio cannot be accurately determined by comparing the peak intensity of the ASE band in the spectrum, as the optical power spectral density of output spectra with different seed linewidths is distinct. Accordingly, the ASE ratio evolution obtained by spectral integration shown in Fig. 7 differs from the ASE peak intensity in the output spectrum of Fig. 6(b). The spectral broadening factor is calculated via dividing the FWHM linewidth of the ns-SFS amplifier by the FWHM linewidth of the ns-SFS seed. As depicted in Fig. 7, the spectral broadening factor decreases rapidly and gradually approaches 1 with the widening of the seed linewidth. This phenomenon can be understood by combining the group-velocity dispersion (GVD) and SPM effects [38]. When the ns-SFS signal has a narrow linewidth, its FWHM linewidth broadens quickly due to SPM. However, the intensity of the GVD effect is highly dependent on the spectral width. Thus, the interplay between the GVD effect and the SPM effect causes the spectrum of the ns-SFS signal with wide linewidth to remain essentially unchanged in the central part at a specific output power. At the same time, the spectral wings will continue to broaden [39].

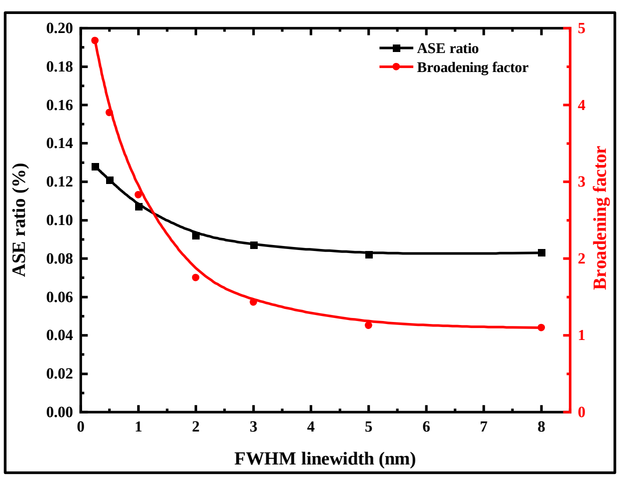

Fig. 7. The dependence of the ASE power ratio and spectral broadening factor on the FWHM linewidth of ns-SFS seed at a pump power of 370 W.

https://doi.org/10.1017/hpl.2023.72 Published online by Cambridge University Press

3.2. The scaling of the output power and pulse energy of filtered ns-SFS seed

According to the above analysis, the filtered ns-SFS seed has an optimal FWHM linewidth to minimize the SRS effect, which is 2 nm in our case, allowing further scaling of the pulse energy and output power of this type of pulsed laser. Therefore, we further amplify the output power and pulse energy of the 2 nm ns-SFS seed after removing the 15 m passive matching fiber in Fig. 3. Through the first booster amplifier, the output power of the 2 nm ns-SFS can be scaled to 1 W, which can be further boosted up to 18 W with the second booster amplifier, thereby delivering adequate signal power for the main amplifier. The dependencies of the average output power and the pulse width of the main amplifier on the pump power are shown in Fig. 8(a). As the pump power increases, the average power grows near linearly, indicating a slope efficiency of 74.1%. However, the pulse width is gradually compressed with the scaling of the pump power due to pulse distortion [31, 40, 41]. As depicted in Fig. 8(b), the leading edge of the pulse consumes more inversion than the trailing edge, resulting in a higher gain and gradual steepening of the leading edge and even causing the pulse compression with the increasing output power. At the maximum pump power of 816.4 W, the pulse duration is narrowed to about 57 ns. Maximum average power of 602 W is achieved, corresponding to a calculated pulse energy of 24.1 mJ and a peak power of 422.5 kW. To our knowledge, this is the highest average power and largest pulse energy ever reported for an all-fiberized narrowband ns-SFS amplifier.

https://doi.org/10.1017/hpl.2023.72 Published online by Cambridge University Press

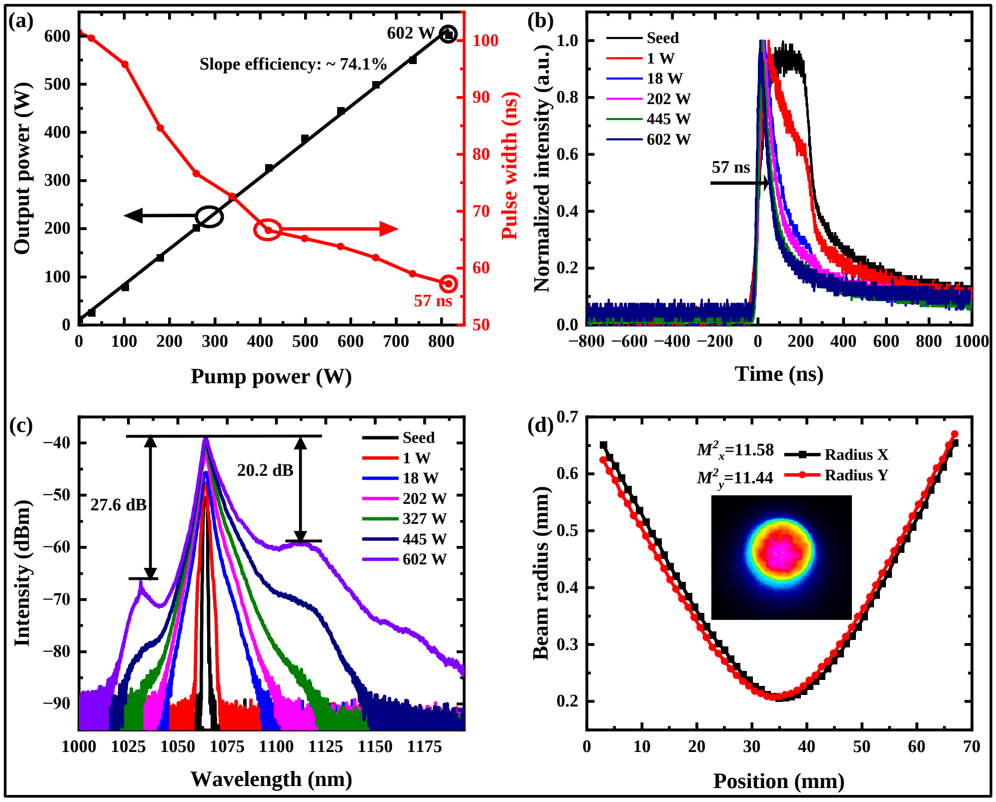

Fig. 8. Output performance of the 2 nm ns-SFS amplifier. (a) Output average power (black line) and pulse width (red line) versus pump power. (b) The pulse profiles at different output powers. (c) The dependence of output spectra on the operation power. (d) The beam quality at the maximum output power of 602 W.

Fig. 8(c) shows the spectra of the amplified 2 nm ns-SFS at different output powers. With the scaling of the output power, the two wings of the spectrum are gradually widened due to the onset of nonlinear effects such as the SPM. At the maximum output power of 602 W, the spectral width widens to 4.1 nm and the central wavelength is 1064.5 nm. The first-order SRS and the second-order SRS wavelength band are suppressed at 20.2 dB and 35 dB, respectively, while the ASE wavelength band is suppressed at 27.6 dB with a weak lasing at 1032 nm. Furthermore, the beam quality at the maximum output power of 602 W is depicted in Fig. 8(d), with the M^2 of approximately 11.51 (M_x^2 =11.58, M_y^2 =11.44). This poor beam quality can be attributed to

https://doi.org/10.1017/hpl.2023.72 Published online by Cambridge University Press

employing the gain fiber with extra-large mode area in the main amplifier. Since the extra-large mode area of the gain fiber supports hundreds of higher-order modes, the mode mixing among these modes makes it difficult to observe the interaction between the fundamental and higher-order modes. Therefore, it is arduous to investigate the nonlinear effects related to the beam quality, such as transverse mode instability and SRS-induced mode distortion in such a large gain fiber [42-44]. Furthermore, enhancing the beam quality of fiber laser systems with high power and large pulse energy is a crucial avenue to unlock their potential applications. The tapered fiber or chirally-coupled-core fiber holds promise in achieving near-diffraction-limited beam quality of such fiber laser systems, while simultaneously addressing challenges such as transverse mode instability and SRS-induced mode distortion.

IV. Conclusion

In conclusion, we first explore the relationship between the SRS effect and the seed' s linewidth of high-power pulsed SFS and find that there is an optimal FWHM linewidth to achieve the lowest SRS for the fiber amplifier. The optimal linewidth is 2 nm in our case, and the first-order SRS power ratio increases rapidly when the seed linewidth deviates from the optimal value. For the ns-SFS seed with a linewidth of less than the optimal value, the intensified fluctuations at the pulse peak result in more severe SRS. On the other hand, for the seed linewidth greater than the optimal width, the wider signal entering the main amplifier contains more Raman band noise than the one at the optimal linewidth and thus causing more severe SRS after power scaling. In addition, by adopting the ns-SFS with a linewidth of 2 nm as the seed, we construct an all-fiberized ns-SFS amplifier with a maximum average power of 602 W and a pulse energy of 24.1 mJ. At the maximum output power, the ns-SFS has a pulse width of 57 ns and a corresponding peak power

https://doi.org/10.1017/hpl.2023.72 Published online by Cambridge University Press

of 422.5 kW. Our study provides valuable insights for further improvements on high-power ns-SFS amplifiers with large pulse energy. Such a laser system offers a promising source for applications such as industrial processing and high-quality full-field imaging of dynamic targets on nanosecond timescales.

Acknowledgement

This work was financially supported by the CAS Project for Young Scientists in Basic Research (No. YSBR-065), the National Natural Science Foundation of China (No. 62225507, No. 62175230, No. U2033211), the Scientific Instrument Developing Project of the Chinese Academy of Sciences (No. YJKYYQ20200001), the National Key R&D Program of China (No. 2022YFB3607800). The authors of this paper would like to thank Professor Jing-yuan Zhang for his precious time and valuable suggestions in the preparation and revision of the manuscript.

References

1. V. Veiko, Y. Karlagina, M. Moskvin, V. Mikhailovskii, G. Odintsova, P. Olshin, D. Pankin, V. Romanov, and R. Yatsuk, "Metal surface coloration by oxide periodic structures formed with nanosecond laser pulses," Opt. Lasers Eng. **96**, 63-67 (2017).
2. T. Heiderscheit, N. G. Shen, Q. H. Wang, A. Samanta, B. X. Wu, and H. T. Ding, "Keyhole cutting of carbon fiber reinforced polymer using a long-duration nanosecond pulse laser," Opt. Lasers Eng. **120**, 101-109 (2019).
3. K. Tsubakimoto, H. Yoshida, and N. Miyanaga, "600 W green and 300 W UV light generated from an eight-beam, sub-nanosecond fiber laser system," Opt. Lett. **42**, 3255-3258 (2017).
4. L. D. Zhang, J. Y. Zhang, X. Wang, M. Tao, G. T. Dai, J. Wu, Z. W. Miao, S. F. Han, H. J. Yu, and X. C. Lin, "Design of coherent wideband radiation process in a Nd3+-doped high entropy glass system," Light-Sci. Appl. **11**, 12 (2022).
5. F. D. Zhang, H. Liu, C. Suebka, Y. X. Liu, Z. Liu, W. Guo, Y. M. Cheng, S. L. Zhang, and L. Li, "Corrosion behaviour of laser-cleaned AA7024 aluminium alloy," Appl. Surf. Sci. **435**, 452-461 (2018).
6. Y. Liu, W. J. Liu, D. Zhang, Z. Q. Tian, X. W. Sun, and Z. Wei, "Experimental investigations into cleaning mechanism of ship shell plant surface involved in dry laser cleaning by controlling laser power," Appl. Phys. A-Mater. Sci. Process. **126**, 17 (2020).
7. L. Huang, P. F. Ma, D. R. Meng, L. Li, R. M. Tao, R. T. Su, Y. X. Ma, and P. Zhou, "Monolithic high-average-power linearly polarized nanosecond pulsed fiber laser with near-diffraction-limited beam quality," High Power Laser Sci. Eng. **6**, e42 (2018).
8. X. C. Chen, N. Wang, C. J. He, and X. C. Lin, "Development of all-fiber nanosecond oscillator using actively Q-switched technologies and modulators," Opt. Laser Technol. **157**, 20 (2023).
9. B. N. Upadhyaya, A. Kuruvilla, U. Chakravarty, M. R. Shenoy, K. Thyagarajan, and S. M. Oak, "Effect of laser linewidth and fiber length on self-pulsing dynamics and output stabilization of single-mode Yb-doped double-clad fiber laser," Appl. Optics **49**, 2316-2325 (2010).

10. W. L. Wang, J. Y. Leng, Y. Gao, S. F. Guo, and Z. F. Jiang, "Influence of temporal characteristics on the power scalability of the fiber amplifier," Laser Phys. **25**, 6 (2015).
11. A. W. Steinforth, J. A. Rivera, and J. G. Eden, "Imaging of transient phenomena with low coherence lasers comprising arrays of independent microbeams: A laser version of Harold Edgerton's stroboscope," APL Phontonics **7**, 11 (2022).
12. J. M. Xu, P. Zhou, W. Liu, J. Y. Leng, H. Xiao, P. F. Ma, J. Wu, H. W. Zhang, J. B. Chen, and Z. J. Liu, "Exploration in Performance Scaling and New Application Avenues of Superfluorescent Fiber Source," IEEE J. .Sel. Top. Quant. **24**(2018).
13. B. Redding, P. Ahmadi, V. Mokan, M. Seifert, M. A. Choma, and H. Cao, "Low-spatial-coherence high-radiance broadband fiber source for speckle free imaging," Opt. Lett. **40**, 4607-4610 (2015).
14. M. Bashkansky, M. D. Duncan, L. Goldberg, J. P. Koplow, and J. Reintjes, "Characteristics of a Yb-doped superfluorescent fiber source for use in optical coherence tomography," Opt. Express **3**, 305-310 (1998).
15. A. J. Jin, H. Zhou, X. F. Zhou, J. Hou, and Z. F. Jiang, "High-Power Ultraflat Near-Infrared Supercontinuum Generation Pumped by a Continuous Amplified Spontaneous Emission Source," IEEE Photonics J. **7**, 1600409 (2015).
16. J. Y. Dong, L. Zhang, H. W. Jiang, X. Z. Yang, W. W. Pan, S. Z. Cui, X. J. Gu, and Y. Feng, "High order cascaded Raman random fiber laser with high spectral purity," Opt. Express **26**, 5275-5280 (2018).
17. J. Storteboom, C. J. Lee, A. Nieuwenhuis, I. D. Lindsay, and K. J. Boller, "Incoherently pumped continuous wave optical parametric oscillator broadened by non-collinear phasematching," Opt. Express **19**, 21786-21792 (2011).
18. X. Cheng, W. W. Pan, X. Zeng, J. Y. Dong, S. Z. Cui, and Y. Feng, "Relative intensity noise comparison of fiber laser and amplified spontaneous emission sources," Opt. Fiber Technol. **54**, 102119 (2020).
19. E. J. Park, J. S. Park, H. Jeong, and J. W. Kim, "High-energy pulsed operation of a Yb fibre master oscillator power amplifier with an amplified spontaneous emission light source," Laser Phys. Lett. **16**, 7 (2019).
20. J. X. Song, H. S. Wu, S. Ren, W. Liu, P. F. Ma, H. Xiao, and P. Zhou, "Comparisons of kilowatt Yb-Raman fiber amplifiers employing a superfluorescent fiber source and fiber oscillator," Opt. Express **29**, 22966-22972 (2021).
21. O. Schmidt, M. Rekas, C. Wirth, J. Rothhardt, S. Rhein, A. Kliner, M. Strecker, T. Schreiber, J. Limpert, R. Eberhardt, and A. Tunnermann, "High power narrow-band fiber-based ASE source," Opt. Express **19**, 4421-4427 (2011).
22. P. F. Ma, L. Huang, X. L. Wang, P. Zhou, and Z. J. Liu, "High power broadband all fiber superfluorescent source with linear polarization and near diffraction-limited beam quality," Opt. Express **24**, 1082-1088 (2016).
23. P. Yan, J. Y. Sun, D. Li, X. J. Wang, Y. S. Huang, M. L. Gong, and Q. R. Xiao, "933 W Yb-doped fiber ASE amplifier with 50.4 nm bandwidth," Opt. Express **24**, 19940-19948 (2016).
24. J. M. Xu, J. Ye, H. Xiao, J. Y. Leng, W. Liu, and P. Zhou, "In-band pumping avenue based high power superfluorescent fiber source with record power andnear-diffraction-limited beam quality," High Power Laser Sci. Eng. **6**, e46 (2018).
25. Z. Li, G. Li, Q. Gao, P. Wu, S. F. She, Z. L. Wang, N. Huang, C. D. Sun, W. Gao, P. Ju, and H. J. Liu, "Kilowatt-level tunable all-fiber narrowband superfluorescent fiber source with 40 nm tuning range," Opt. Express **28**, 10378-10385 (2020).
26. J. Ye, C. C. Fan, J. M. Xu, H. Xiao, J. Y. Leng, and P. Zhou, "2-kW-level superfluorescent fiber source with flexible wavelength and linewidth tunable characteristics," High Power Laser Sci. Eng. **9**, e55 (2021).
27. C. Jauregui, J. Limpert, and A. Tunnermann, "High-power fibre lasers," Nat. Photonics **7**, 861-867 (2013).
28. T. Schreiber, A. Liem, E. Freier, C. Matzdorf, R. Eberhardt, C. Jauregui, J. Limpert, and A. Tunnermann, "Analysis of stimulated Raman scattering in cw kW fiber oscillators," in *Conference on Fiber Lasers XI - Technology, Systems, and Applications*, Proceedings of SPIE (Spie-Int Soc Optical Engineering, 2014), 89611T.
29. W. Liu, P. F. Ma, H. B. Lv, J. M. Xu, P. Zhou, and Z. F. Jiang, "Investigation of stimulated Raman scattering effect in high-power fiber amplifiers seeded by narrow-band filtered superfluorescent source," Opt. Express **24**, 8708-8717 (2016).
30. V. Bock, A. Liem, T. Schreiber, R. Eberhardt, and A. Tunnermann, "Explanation of Stimulated Raman Scattering in high power fiber systems," in *Conference on Fiber Lasers XV - Technology and Systems*, Proceedings of SPIE (Spie-Int Soc Optical Engineering, 2018), 105121F.

https://doi.org/10.1017/hpl.2023.72 Published online by Cambridge University Press

31. C. Y. Ning, S. Z. Zou, H. J. Yu, S. Xu, X. C. Chen, J. X. Zuo, S. F. Han, X. Y. Li, Z. Y. Zhang, C. J. He, and X. C. Lin, "Monolithic all-fiberized nanosecond laser with kilowatt average power and megawatt peak power," Opt. Laser Technol. **157**, 9 (2023).
32. W. Liu, P. F. Ma, H. B. Lv, J. M. Xu, P. Zhou, and Z. F. Jiang, "General analysis of SRS-limited high-power fiber lasers and design strategy," Opt. Express **24**, 26715-26721 (2016).
33. W. Liu, P. F. Ma, P. Zhou, and Z. F. Jiang, "Optimization for the fiber laser source through its temporal and spectral characteristics," in *Conference on High-Power Lasers - Technology and Systems, Platforms, and Effects*, Proceedings of SPIE (Spie-Int Soc Optical Engineering, 2017), 104360O.
34. J. Ye, X. Y. Ma, Y. Zhang, J. M. Xu, H. W. Zhang, T. F. Yao, J. Y. Leng, and P. Zhou, "Revealing the dynamics of intensity fluctuation transfer in a random Raman fiber laser," Photonics Res. **10**, 618-627 (2022).
35. X. L. Shen, H. T. Zhang, H. Hao, D. Li, P. Yan, and M. L. Gong, "Self-phase modulation of nanosecond pulses in fiber amplifiers with gain saturation," Opt. Express **24**, 4382-4390 (2016).
36. W. Liu, S. Ren, P. F. Ma, and P. Zhou, "Impact of amplified spontaneous emission noise on the SRS threshold of high-power fiber amplifiers," Chin. Phys. B **32**, 5 (2023).
37. H. Y. Ying, J. Q. Cao, Y. Yu, M. Wang, Z. F. Wang, and J. B. Chen, "Raman-noise enhanced stimulated Raman scattering in high-power continuous-wave fiber amplifier," Optik **144**, 163-171 (2017).
38. D. B. S. Soh, J. P. Koplow, S. W. Moore, K. L. Schroder, and W. L. Hsu, "The effect of dispersion on spectral broadening of incoherent continuous-wave light in optical fibers," Opt. Express **18**, 22393-22405 (2010).
39. W. Liu, P. F. Ma, P. Zhou, and Z. F. Jiang, "Spectral property optimization for a narrow-band-filtered superfluorescent fiber source," Laser Phys. Lett. **15**, 6 (2018).
40. L. M. Frantz and J. S. Nodvik, "Theory of pulse propagation in a laser amplifier," J. Appl. Phys. **34**, 2346-& (1963).
41. D. N. Schimpf, C. Ruchert, D. Nodop, J. Limpert, A. Tunnermann, and F. Salin, "Compensation of pulse-distortion in saturated laser amplifiers," Opt. Express **16**, 17637-17646 (2008).
42. C. Jauregui, C. Stihler, and J. Limpert, "Transverse mode instability," Adv. Opt. Photonics **12**, 429-484 (2020).
43. V. Distler, F. Moller, B. Yildiz, M. Plotner, C. Jauregui, T. Walbaum, and T. Schreiber, "Experimental analysis of Raman-induced transverse mode instability in a core-pumped Raman fiber amplifier," Opt. Express **29**, 16175-16181 (2021).
44. Q. H. Chu, Q. Shu, Z. Chen, F. Y. Li, D. L. Yan, C. Guo, H. H. Lin, J. J. Wang, F. Jing, C. X. Tang, and R. M. Tao, "Experimental study of mode distortion induced by stimulated Raman scattering in high-power fiber amplifiers," Photonics Res. **8**, 595-600 (2020).

https://doi.org/10.1017/hpl.2023.72 Published online by Cambridge University Press

Figures and tables

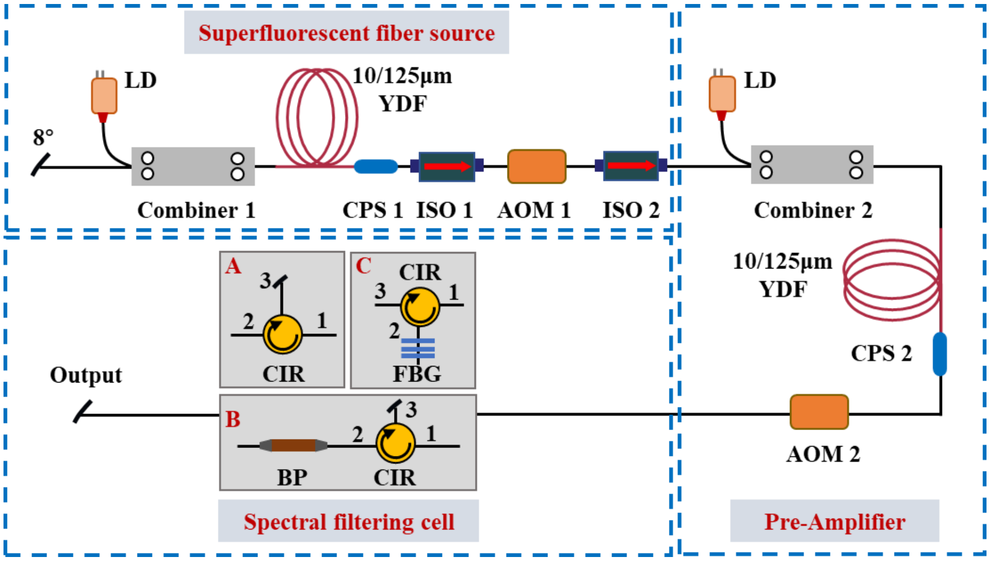

Figure 1

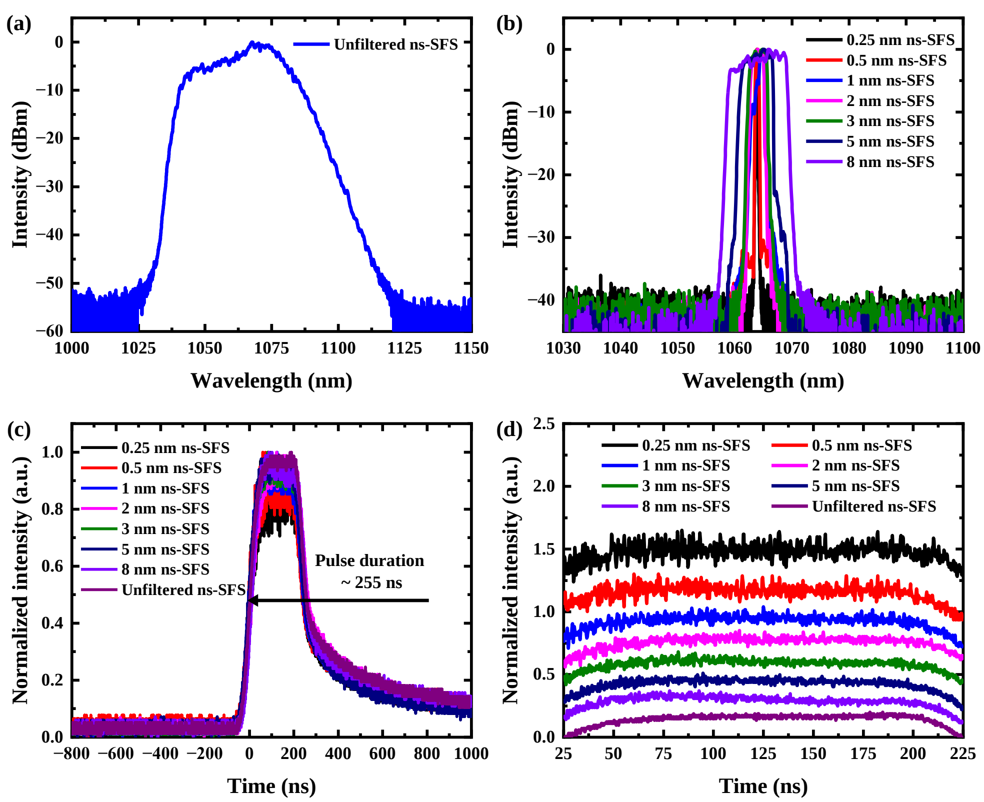

Figure 2

https://doi.org/10.1017/hpl.2023.72 Published online by Cambridge University Press

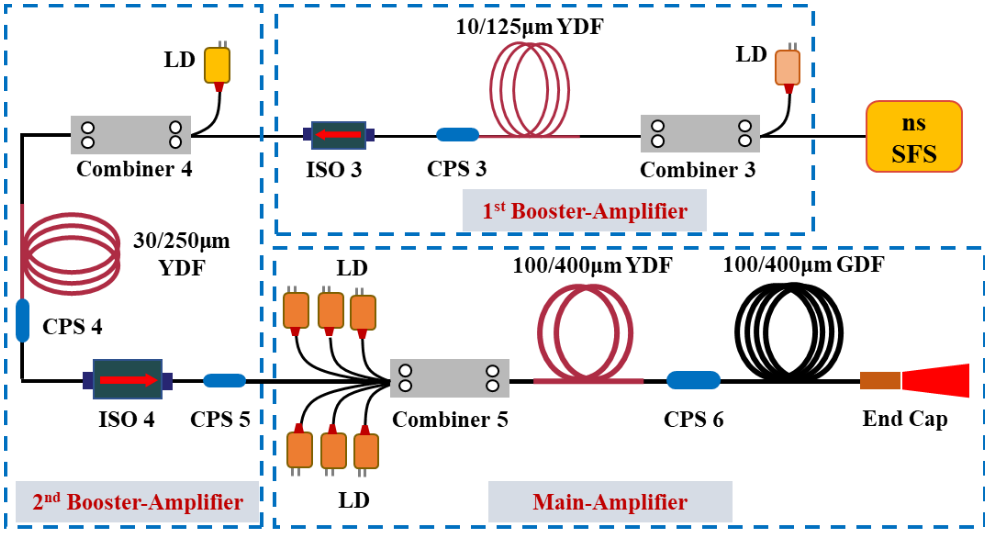

Figure 3

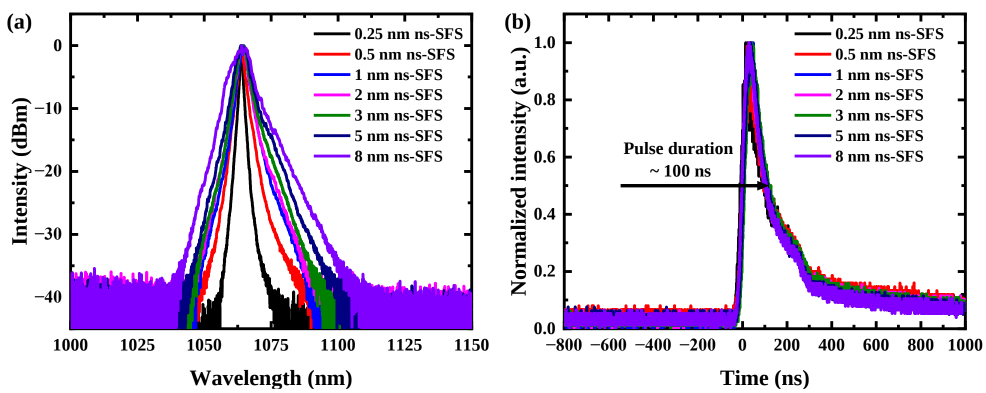

Figure 4

https://doi.org/10.1017/hpl.2023.72 Published online by Cambridge University Press

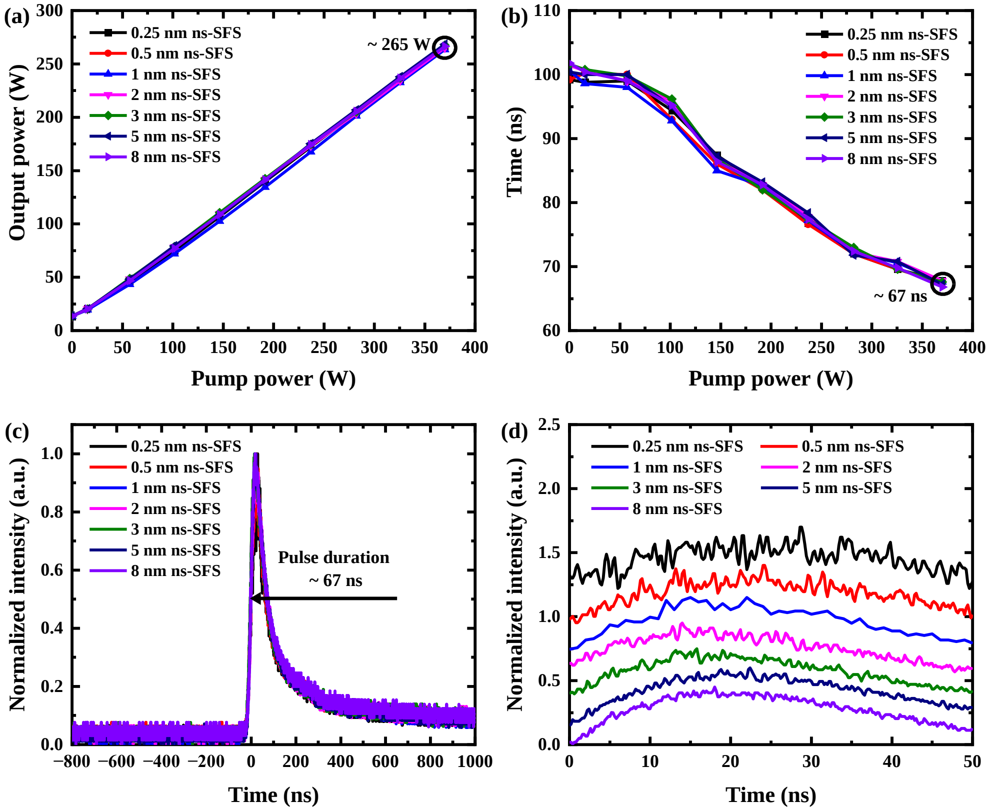

Figure 5

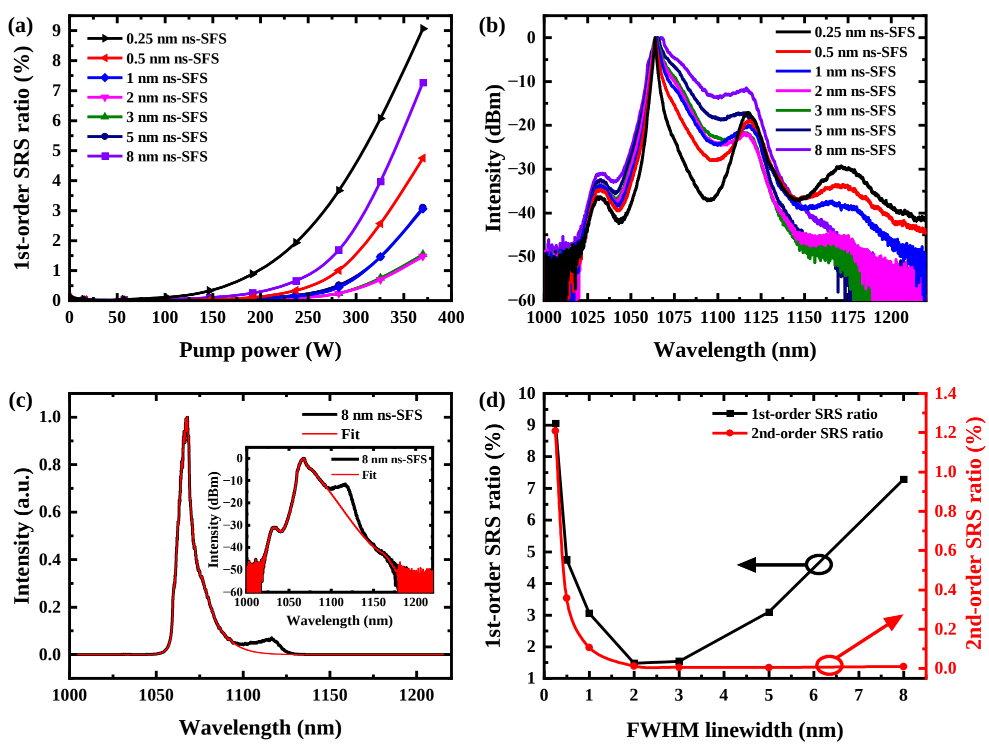

Figure 6

https://doi.org/10.1017/hpl.2023.72 Published online by Cambridge University Press

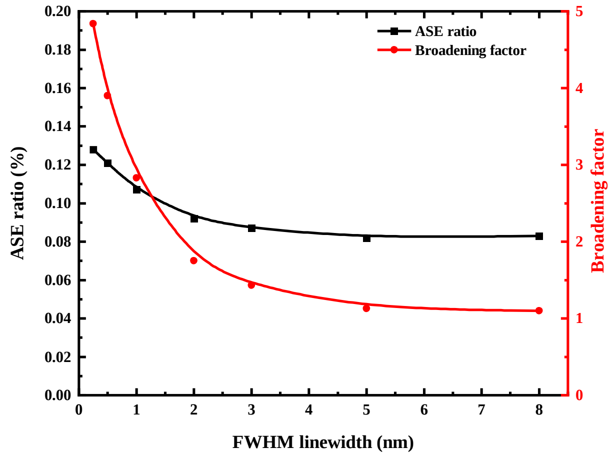

Figure 7

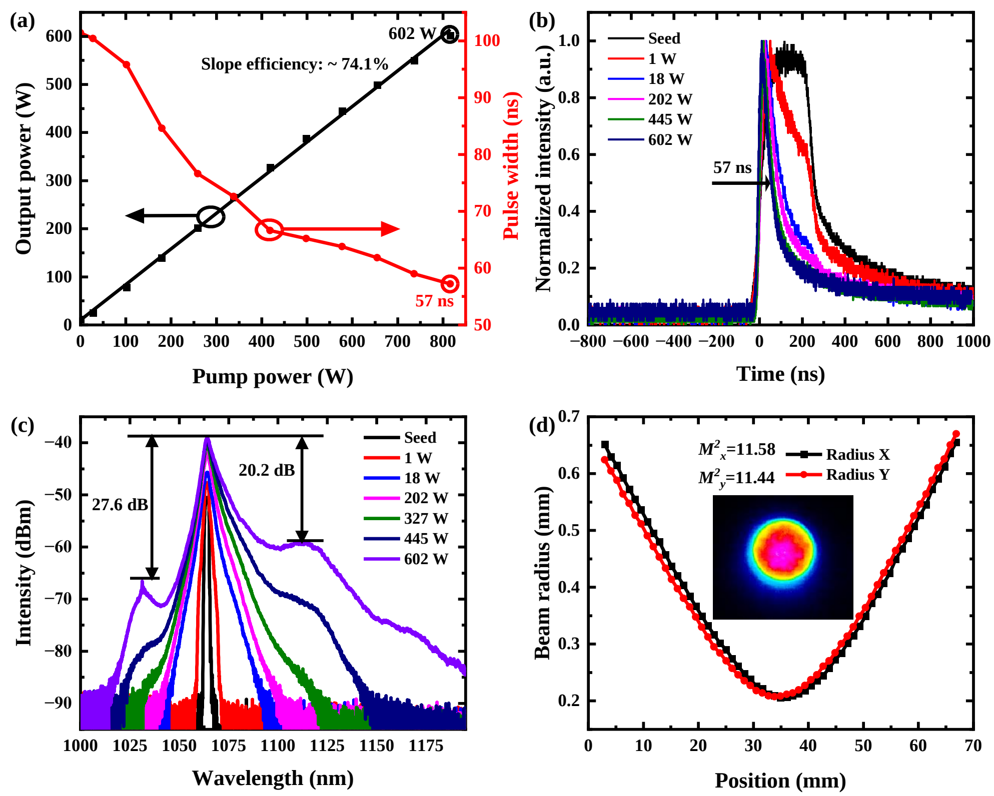

Figure 8

https://doi.org/10.1017/hpl.2023.72 Published online by Cambridge University Press

Table 1

Seed linewidth (nm)	Output power (mW)	Seed linewidth (nm)	Output power (mW)
unfiltered ns-SFS	445.0	2	22.4
8	133.1	1	11.5
5	36.6	0.5	5.7
3	30.8	0.25	3.0

https://doi.org/10.1017/hpl.2023.72 Published online by Cambridge University Press

Figure and table captions

Figure 1. The experimental setup of the ns-SFS seed.

Figure 2. The output characteristics of ns-SFS seed. The output spectra of the unfiltered ns-SFS (a) and the filtered ns-SFSs (b). (c) The pulse profiles, and (d) the fluctuations at the pulse peak of the ns-SFS seed.

Figure 3. The experimental setup of ns-SFS amplifier.

Figure 4. The output spectra (a) and the pulse profiles (b) of the ns-SFS signals at an output power of ~ 18 W.

Figure 5. (a) The output power and (b) pulse width of amplified ns-SFS signals as a function of pumping power, (c) the pulse profiles, and (d) the details of the pulse peak of amplified ns-SFS signals at a pump power of 370 W.

Figure 6. The SRS of amplified ns-SFS with various linewidths. (a) The first-order SRS power ratio of seven ns-SFS amplifiers under different pump powers. (b) The output spectra of the ns-SFS amplifiers with a pump power of 370 W. (c) The experimental and fitted output spectra in the case of 8 nm ns-SFS at a pump power of 370 W in a linear scale, insert: the corresponding spectra in a logarithmic coordinate. (d)The first-order SRS power ratio and the second-order SRS power ratio versus the ns-SFS seed' s FWHM linewidth at a pump power of 370 W.

Figure 7. The dependence of the ASE power ratio and spectral broadening factor on the FWHM linewidth of ns-SFS seed at a pump power of 370 W.

Figure 8. Output performance of the 2 nm ns-SFS amplifier. (a) Output average power (black line) and pulse width (red line) versus pump power. (b) The pulse profiles at different output powers. (c) Output spectra dependence on the operation power. (d) The beam quality at the maximum output power of 602 W.

Table 1. Output power of ns-SFS seed vs. FWHM linewidth

https://doi.org/10.1017/hpl.2023.72 Published online by Cambridge University Press